Solar Energy Materials & Solar Cells 262 (2023) 112540

Contents lists available at ScienceDirect

Solar Energy Materials and Solar Cells

journal homepage: www.elsevier.com/locate/solmat

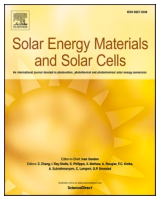

Stability of black interconnect coatings for solar photovoltaic module applications

Alejandro Borja Block [a,*], Chiara Barretta [b], Antonin Faes [a,c], Alessandro Virtuani [c], Aleš Vlk [d], Martin Ledinský [d], Gernot Oreski [b], Christophe Ballif [a,c]

[a] École Polytechnique Fédérale de Lausanne (EPFL), Institute of Electrical and Micro Engineering (IEM), Photovoltaics and Thin-Film Electronics Laboratory (PV-Lab), Rue de la Maladière 71b, 2002, Neuchâtel, Switzerland
[b] Polymer Competence Center Leoben GmbH (PCCL), Roseggerstrasse 12, 8700, Leoben, Austria
[c] CSEM, Sustainable Energy Center, Rue de Jaquet-Droz 1, 2002, Neuchâtel, Switzerland
[d] Laboratory of Nanostructures and Nanomaterials, Institute of Physics, Academy of Sciences of the Czech Republic, Prague, 162 00, Czech Republic

ARTICLE INFO

Keywords:
Photovoltaics
Black metallic ribbons
Ink
Yellowing
Photodegradation
2-Phenoxyethyl acrylate

ABSTRACT

Building-integrated photovoltaics (BIPV) are dual purpose, providing both energy and building functions. Aesthetics play a crucial role in the BIPV market, with increasing demand for uniformly colored modules for building skins. Achieving this requires hiding ribbons and metal connections while not compromising durability, and ink coating offers a potential automated solution. This work presents a comparison of three coated metallic ribbons: one commercially pre-coated and two coated with UV-curable-inkjet printing. Glass/backsheet samples with standard or UV-blocking encapsulant were tested through accelerated ageing UV exposure. Results show that the commercially coated ribbons remain stable after 120 kWh/m^2 of UV, but the UV-curable-inkjet tested inks show color changes in the encapsulant surrounding metallic interconnects in all cases. Yellowing is attributed to photodegradation of the ink's #1 main component, 2-phenoexyethyl-acrylate. However, PV module performance remains stable despite the color shift, with less than 3% power loss after exposure to 360 kWh/m^2 of UV.

1. Introduction

Climate change is one of the most pressing challenges facing our society today, and the building sector is a major contributor to greenhouse gas emissions. Buildings account for around 30% of global energy consumption and approximately one-third of global CO_2 emissions [1]. Building-integrated photovoltaic (BIPV) modules can be incorporated into the building envelope, for example on roofs, facades, and windows, to generate electricity while also providing shade, insulation, and other benefits. By generating electricity from renewable sources, buildings can reduce their dependence on fossil fuels and help mitigate the environmental impacts associated with traditional energy production [2].

BIPV modules can be designed in a range of shapes, sizes, and colors, enabling architects and designers to create visually stunning and energy-positive buildings. One important factor for BIPV acceptance by architects and house owners is the aesthetic of the active PV construction elements. In particular, the homogenous appearance is of high importance even if the performance is reduced.

The overall appearance of the modules, created by the mix of dark cells, metallic ribbons, and typically white backsheets, is frequently perceived as visually unappealing, complicating PV incorporation in the built environment [3]. In many cases, BIPV modules are still considered a non-aesthetic appendage by architects. As aesthetic is still a crucial point in the consumer decision of purchase [4], in recent years, several BIPV module manufacturers have attempted to mask the highly reflective metallic interconnects to minimize inhomogeneous patterns of solar modules and used black backsheets in place of white ones.

Metallic ribbons, connectors or interconnects play an important role in the construction of PV modules. These thin strips of metal are used to connect the individual solar cells in the module, allowing the current to flow from cell to cell and ultimately to the external electrical circuit. In addition to their functional role in the module, metallic ribbons can also contribute to its aesthetic appeal. Interconnect hiding is often achieved through expensive and inefficient manufacturing steps, such as applying colored strips or bands with manual positioning. A possible solution to modify the appearance of the metallic ribbons is to coat them with ink. However, the metallic ribbons come in different shapes, orientations, and sizes, depending on the module design and solar cells used;

* Corresponding author.
E-mail address: alejandro.borjablock@epfl.ch (A. Borja Block).

https://doi.org/10.1016/j.solmat.2023.112540
Received 29 June 2023; Received in revised form 7 August 2023; Accepted 30 August 2023
Available online 23 September 2023

therefore, coating them is not straightforward. Inkjet is one of the best technologies able to cope with the requirements of accuracy, resolution, and flexibility to coat the bright metallic ribbons, even on top of the solar cells.

Ink coated metallic ribbons could be a suitable solution to achieve the uniform appearance architects seek. Nevertheless, using ribbons pre-coated with black color on the production line has many challenges. They are stretched, bent, soldered and laminated at high temperatures (>300 °C and ~150 °C respectively), all of which the black coating should withstand while maintaining the production line speed. An alternative solution will be the coating of the interconnects by advanced inkjet printing after the stringing and soldering of the solar cell array. The curing of the ink should be fast, making UV curable inks an appropriate candidate.

UV-curable inkjet inks are typically made of a mixture of monomers, oligomers, photoinitiators, colorants, and additives. These materials are well described by S. Magdassi et al. [5]. Monomers are small molecules that form the polymer backbone of the ink when exposed to UV light. Oligomers are larger molecules that polymerize to control the physical properties of the cured ink, such as hardness and flexibility. Photo-initiators are chemicals that are sensitive to UV light and are added to the ink to initiate the polymerization process when exposed to UV light. Colorants (e.g. pigments or dyes) are added to provide color to the ink, and additives such as surfactants and stabilizers are used to improve the ink's performance and stability. UV-curable inkjet inks can be formulated to work with a wide range of substrates, including paper, plastics, glass, metal, and ceramics, and can be customized for specific printing applications. However, there are many considerations to be taken into account when formulating a UV-curable inkjet ink (e.g. viscosity, surface tension, particle size, colorant type, cure speed, etc.) [6]. No UV-curable inkjet inks are specifically made for BIPV applications. To be compatible with PV applications, the ink should first wet and have good printing quality on cell and string interconnects, and then it should have strong adhesion not to be delaminated due to the shear stresses in the encapsulants during module lamination, ruining the aesthetic appearance. Finally, the ink should have long term stability as PV modules are subjected to long-term exposure weather stressors including humidity, temperature, and light, which are known to cause deterioration of polymer module materials such as backsheets and encapsulants [7].

Little is known about the stability of black ribbons in these conditions and the effects the black coatings could create in the PV modules. The components of the black ink could react with the materials of the PV modules and produce degradation. To date there are no specific requirements for colored ribbons for PV applications besides the common qualification tests used for PV modules such as IEC 61215 [8]. Few studies have tested the stability and requirements of black metallic ribbons for integrated PV applications [9–11]. The objectives of this research are to determine whether the black coatings are stable after a protocol based on UV light exposure tests for polymeric materials used by the PV industry [12], discuss the challenges of these products and understand the degradation mode observed focusing on a particular ink, exhibiting the most substantial color change among the tested samples.

2. Material and methods

We selected three different black metallic ribbons. One was commercially-available but with no information about the used coating, while the other two were coated in the laboratory with UV-curable inkjet commercial inks (see Table I). The only available information for the inks used was the safety datasheet. One key advantage of inkjet UV-curable coated ribbons was their ability to be coated immediately after the soldering process. This eliminated the need for the coatings on metallic ribbons to withstand high temperatures, thereby avoiding any potential damage or degradation caused by extreme heat.

Depending on the compatibility of the inkjet equipment, the ribbons were coated manually or according to the dispensing technique suggested by the distributor. The curing process was carried out for ink #1 and #2 using a FireJet One UV 20 W lamp emitting at 395 nm with 4 passes at 100 mm/s with a substrate distance of 3 mm. The samples were subjected to light and temperature exposure according to IEC 62788-7-2 [12]. Assessing the stability of the coatings was necessary to understand the effect they will have on the PV module in the long-term. The characterization was performed with image processing visual inspection on all the samples.

Table 1
Black metallic ribbons investigated in this work. The initial two ribbons were coated with UV-curable inkjet ink, whereas the third ribbon was a commercially available black pre-coated metallic ribbon with a dispensing technique and ink that were not specified. All materials are commercially available components.

Metallic ribbon #	Type	Dispensing technique	Ink info	Ribbon info
1	UV curable	Inkjet	Safety datasheet	Copper with Sn: Pb = 70:30-60:40 coating
2	UV curable	Inkjet	Safety datasheet	Copper with Sn: Pb = 70:30-60:40 coating
3	Unknown	Unknown	Technical specification	Copper with Sn: Pb = 70:30-60:40 coating

A deeper study was carried out only with the ink that was known to produce the largest color change (ink #1) in one-solar cell PV modules according to previous investigation [11], and due to the challenge of investigating commercial components with undisclosed materials. The characterization techniques employed were attenuated total reflectance Fourier transform infrared spectroscopy (ATR-FTIR), UV-fluorescence imaging, thermo-desorption gas chromatography coupled to mass spectrometry (TD-GCMS) and Raman spectroscopy. Single solar cell mini-modules were manufactured employing ink #1 with the help of a laboratory-designed ribbon coating equipment to mask all the metallic ribbons, even the cell connectors at the top of the solar cell. The one solar cell mini modules were also exposed to the same protocol to assess, through electrical performance measurements (IV curve and electroluminescence), the effects of unstable coatings on PV modules.

2.1. Sample preparation

The stability and performance of the inks was tested on three levels under UV exposure (see Table II): 1) Glass–backsheet (G/BS) laminates to investigate the interactions of all the inks with the encapsulants. 2) Individual ink #1 components to check the potential root causes for color change, because ink #1 produced the largest visual modifications. 3) Coated one solar cell PV modules to investigate the influence of ink #1 on the electrical performance.

2.1.1. G/BS laminates

After coating, the metallic ribbons were cut into 3 cm long stripes. They were then laminated at around 150 °C in the conventional PV configuration glass-backsheet (G/BS) using solar glass (see Fig. 1). Three different types of encapsulants were chosen, one made of ethylene vinyl acetate (EVA) and the other two based on polyolefin elastomer (POE), with and without UV blockers. The encapsulant with UV blockers had a

Table 2
UVA + UVB dose applied to each sample in this work. Three different kinds of samples were used: G/BS coupons with coated ribbons and with ink components, pure ink components in small glass bottles and mini modules.

Sample	UVA + UVB dose (kWh/m^2)
G/BS coupons	120
Pure ink components	1.5 and 15
One solar cell PV modules	360

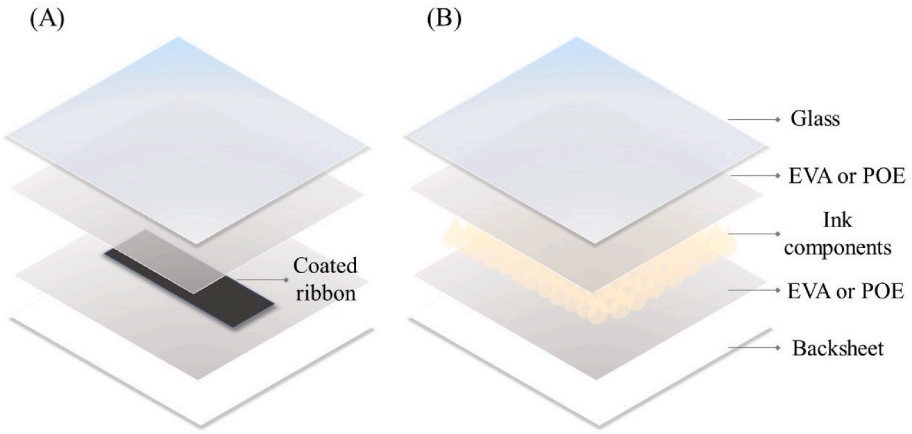

Fig. 1. Typical sample configuration manufactured in this investigation. They were produced with either EVA or POE with or without UV blocker. (A) Sample with encapsulated coated ribbon, this type of sample was manufactured with all inks. (B) Sample with ink component, this type of sample was manufactured only with ink #1.

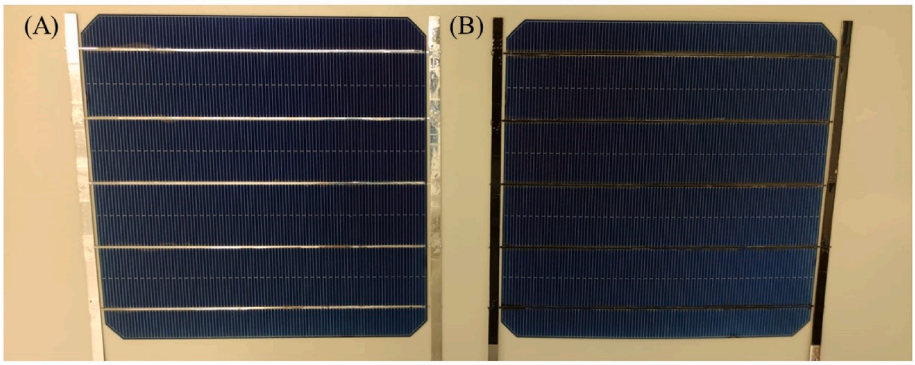

Fig. 2. (A) Solar cell with uncoated ribbons and (B) solar cell with black coated ribbons. The high reflection of the uncoated ribbons can be observed.

transmittance of equal to or less than 30% for wavelengths ranging from 290 nm to 380 nm, while those without UV blockers had larger transmittance than 70% in the same range. The idea of comparing an encapsulant with UV blockers with encapsulant without UV blockers came from the hypothesis that they could mitigate the degradation observed with unstable inks. The final size of the G/BS laminates were 5 cm × 5 cm. Glass-glass (G/G) samples were not manufactured since recent investigations into G/G and G/BS samples showed similar effects after light exposure [9,11]. Furthermore, G/BS samples had the crucial advantage that they can be peeled to have access to the materials inside the laminates for further characterization (see Fig. 2).

Our study primarily centered on ink #1 to investigate the significant color change observed in this particular ink. Inks are complex mixtures containing various interacting substances, including undisclosed materials. To simplify our research, we generated samples similar to those depicted in Fig. 1(B). Instead of using coated metallic ribbons, we laminated either ink flush or pure monomers droplets of ink #1 between the encapsulants. Ink flush is a liquid product designed for printhead maintenance and ink cleaning. In the case of ink #1, the primary component of the ink flush matches the main component of the ink itself, which is 2-phenoxyethyl acrylate (2-PEA). In this study, the ink flush and pure component primarily consisted of 2-phenoxyethyl acrylate. However, it's important to note that ink flush is not as pure as the standalone component. The decision to use ink flush was based on logistical considerations and material availability. Furthermore, we replicated the same samples by laminating pure 2-PEA in the G/BS configuration, as depicted in Fig. 1(B).

2.1.2. Pure component degradation

As previously mentioned, the inks are made with several components (i.e. monomers, oligomers, photoinitiators, colorants, and additives) that interact between themselves and with the materials of the substrate and surroundings. We isolated in small glass bottles the ink flush #1 and the pure molecule 2-PEA to investigate whether it played an important role on the degradation observed.

2.1.3. Coated solar cell mini modules

We investigated the effect of the ink #1 on a one solar cell G/BS mini module. Samples were prepared by first soldering the cell, subsequently the ribbons were coated with the help of the laboratory-developed inkjet ribbon-coating equipment that can coat ribbons even on top of the solar cells. The equipment consists of a customized inkjet printer specifically designed for coating laboratory samples. However, it offers scalability possibilities to industrial scale, allowing for the modification of the appearance of PV modules. It employs high-resolution actuators and image processing to detect cell connectors and interconnects with remarkable precision. After coating, the stringed solar cell was encapsulated and laminated with front solar glass, EVA, and a rear black backsheet. This was also performed with an uncoated cell. The goal of these samples was to investigate the effect of an ink that produces large color change on a PV module.

2.2. Testing sequence

The samples followed a sequence based on IEC 62788-7-2 standard with A3 conditions [12]. They were placed inside a Q-Sun Xenon

chamber (Q-SUN Model Xe-3) with a noon summer sunlight filter following the conditions of Table III.

The G/BS coupons were left in the chamber for a total of 2000 h, equivalent to roughly 120 kWh/m^2 of UVA + UVB, which corresponds approximately to 2 years of outdoor exposure in central Europe. The mini modules were aged for a total of 6000 h, and the pure component samples simply for 24 h and 10 days. This was because the degradation observed appeared very rapidly. The total UV dose was presented in Table 2.

2.3. Characterization techniques

The measurements performed in this work aim to assess the effects of the coatings in common PV materials under accelerated aging tests. In the case of PV modules, these impacts can be both aesthetic and on the electrical performance.

2.3.1. Visual and UV-fluorescence imaging

Images of the samples were taken periodically with high illumination and resolution using a scanner machine. A software was developed using image processing to compare the RGB color coordinates' change in the sample previous to and after UV exposure, employing the CIEDE2000 formula [13]. While the sample is deteriorating, the program allows a relative change in color to be observed and calculated. Less stable inks will exhibit a greater color change (ΔE). Further images were taken with UV-fluorescence imaging with a 365 nm UV LED flood light and a digital camera to assess polymer degradation [14].

2.3.2. Attenuated total reflectance fourier transform infrared spectroscopy (ATR-FTIR)

The G/BS laminates were peeled manually, and the chemical changes in the encapsulant and pure ink components were assessed with attenuated total reflectance (ATR) Fourier transform infrared (FTIR) spectroscopy. A Bruker Vertex 80 spanning the 400-4000 cm^{-1} range with 64 scans in absorbance mode was used to collect the data. The background was collected on a clean ATR diamond crystal. Several measurements of each sample were taken in various spots and the data was then processed and normalized. The same process was followed with the polymerized pure ink components. The carbonyl index was calculated as shown in Equation (1) [15,16]:

$$Carbonyl\ Index\ (\%) = \frac{I_{1720}}{I_{2920}} \times 100 \quad (1)$$

2.3.3. Thermo-desorption gas-chromatography coupled to mass-spectrometry (TD-GCMS)

The method was used to analyze the chemical processes that occur in samples containing ink 1# components. About 1 mg of reference and contaminated encapsulant with ink component materials were extracted from the G/BS laminates to qualitatively investigate the changes in the additive composition and formation of possible degradation products that took place during exposure. TD-GCMS experiments were carried out using a GC-MS QM2010 Ultra from Shimadzu equipped with a Pyrolyzator 3030D from Frontier laboratories. The encapsulant samples were heated up in the furnace of the pyrolyzator from 60 °C to 320 °C with a heating rate of 20 °C/min and kept at 320 °C for 3 min. The gases evolving from the encapsulants during this step were then carried into the GC using helium as carrier gas. The evolved substances were separated in the GC equipped with an Optima-5-Accent column, with length of 30 m and inner diameter of 0.25 mm. The interface between GC and pyrolyzator was kept at 300 °C, and thermal protocol in the GC was characterized by the following steps: (I) heating from 50 °C to 90 °C with a heating rate of 10 °C/min, (II) isotherm at 90 °C for 2 min, (III) heating from 90 °C to 300 °C with a heating rate of 10 °C/min, (IV) isotherm at 300 °C for 10 min. Each substance eluting from the column was then ionized using an ionization energy of 70 eV and mass spectra were recorded in the range of *m/z* 50 – 800. The identification of the mass spectra was carried out by comparison with the NIST database.

Table 3
Test conditions in the UV chamber according to IEC 62788-7-2 standard with A3 conditions.

Condition	Value
Irradiance	0.8 W/ m^2 at 340 nm
Relative humidity	20%
UV intensity (UV-A + UV-B)	~60 W/ m^2
Chamber air temperature	65 °C
Black panel temperature	90 °C

2.3.4. Raman spectroscopy

Similarly, as ATR-FTIR, the G/BS laminates were peeled manually, and the chemical changes in the encapsulant were assessed. The Raman spectra were acquired using two Renishaw InVia confocal spectrometer using 785 nm laser as excitation source. Line map of the Raman spectra of the sample was taken using 100x Leica objective (numerical aperture NA = 0.90), dielectric rejection filter, and 1200 groves/mm diffraction grating. As a calibration sample, Raman line of crystalline silicon at 520.5 cm^{-1} was used.

2.3.5. IV curve and electroluminescence (EL)

The one-sun IV curve and electroluminescence (EL) were measured on single solar cell mini modules to determine the difference between coated and uncoated PV modules after UV exposure. Standard tests conditions (25 °C, Air Mass 1.5g, 1000 W/m^2) were followed with irradiance and temperature calibration correction using a PASAN solar simulator.

3. Results and discussion

The results are divided in five main sections. The first section examines the results of the digital images, color change and UV-fluorescence imaging. The second, third, and fourth includes the characterization of the investigated samples with ATR-FTIR, TD-GCMS, and Raman spectroscopy, respectively. Finally, the electrical performance of the mini modules is assessed.

3.1. Visual inspection

The G/BS laminates were scanned at 0 kWh/m^2 and at 120 kWh/m^2. Fig. 3 presents the results of the color change (ΔE) from the samples previous to and after degradation. Different encapsulants (e.g EVA or POE) showed no major effect on the color change perceived. The single most striking observation to emerge from the data comparison was that the color change only appeared on the UV curable inkjet inks, while not on the commercial black ribbons.

Ink #1 produced the largest color change, a yellow halo in the surroundings of the coated metallic interconnects appeared. This could indicate diffusion of ink components into the encapsulant and degradation. Ink #2 produced a milder but still noticeable color change. No increase in ΔE was detected for ink #3. Surprisingly, the UV blocker encapsulant did not mitigate the color change effect for the black coatings in any case.

The G/BS laminates containing 2-PEA were photographed at ambient light and with UV-fluorescence imaging to compare exposed and not exposed samples. Fig. 4 shows the difference, while with ambient light all samples appear white (since the backsheet is white colored) with UV light an evident fluorescence is observed for the encapsulants without UV blockers. After exposure there might be chromophore formations in the 2-PEA component that produce fluorescence under UV light [17].

On samples with UV blockers, no color change was found. This suggests that encapsulants with UV blockers help preserving the major

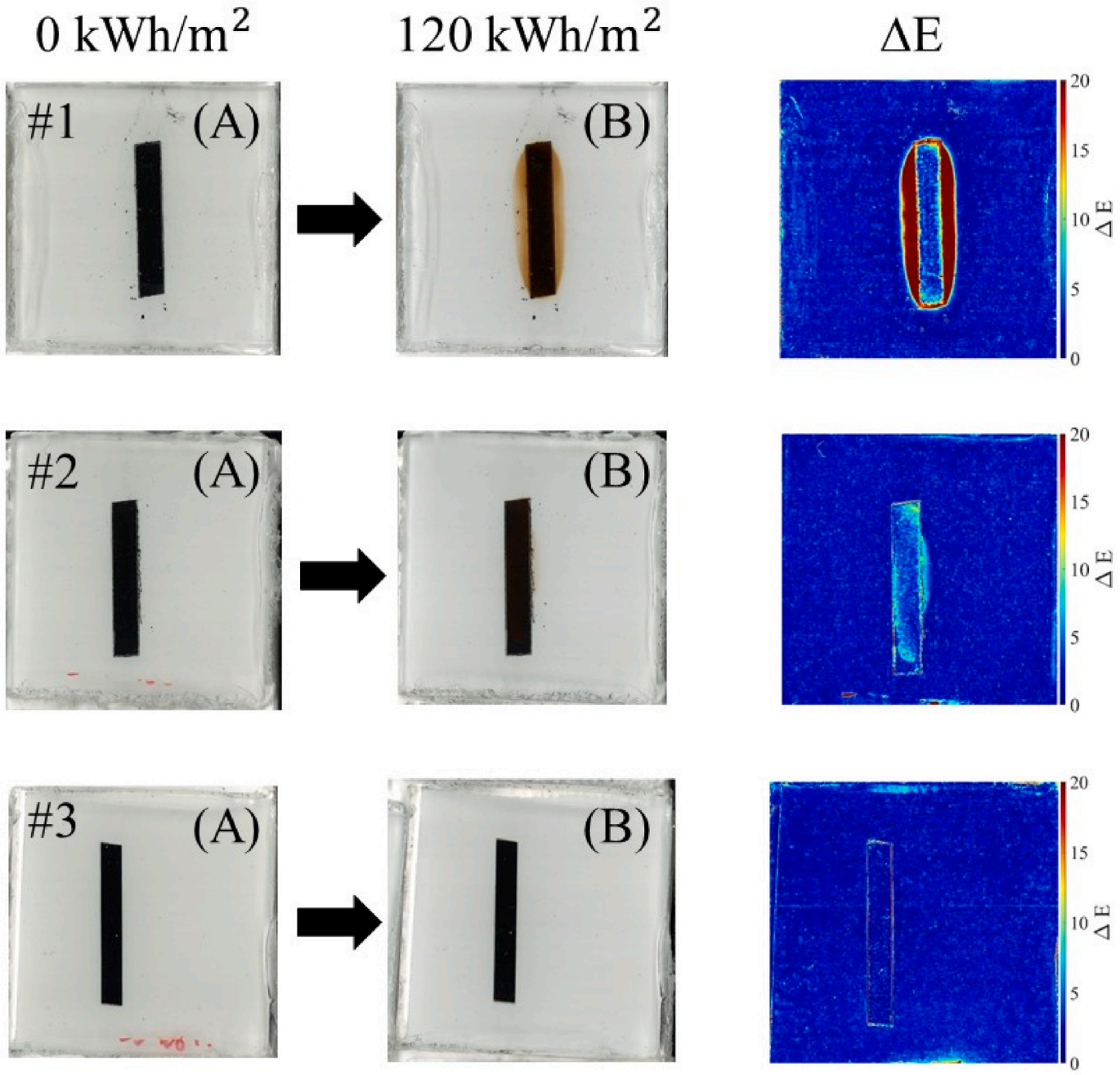

Fig. 3. G/BS laminates before and after UV exposure for all studied inks (#1, #2 and #3). On the right, the image depicting a value of color change for each pixel between the two images. The image is generated by aligning image (A) and (B) to then calculate the color change (ΔE) between them. (#1) Ink #1 made mainly of 2-PEA produces a yellow halo after 120 kWh/m^2 of UV exposure. (#2) UV curable ink #2 produces a mild but still noticeable color change. (#3) Commercial pre-coated metallic ribbon is stable after 120 kWh/m^2 of UV exposure.

component of ink #1 (2-PEA). Even with UV blockers, yellowing happened in samples with coated metallic interconnects. This phenomenon might be explained by the deterioration of another ink components, potentially with greater light wavelength exposure, temperature or humidity.

3.2. Attenuated total reflectance fourier transform infrared spectroscopy (ATR-FTIR)

The peeled G/BS laminates and pure components were measured. In the case of the samples encapsulated with flush clear peaks corresponding to the 2-PEA appeared in the range of 1300 to 1100 cm^{-1} (see Fig. 5). After the exposure of 120 kWh/m^2 of UV, no difference was appreciated in the ATR-FTIR spectra even when a change in color was observed for the sample with flush. The reference samples (samples without any ink component) did not show any major change in the spectra after exposure. The same effect happened with all encapsulants tested. The same measurement was performed on the samples with coated metallic ribbons, but no difference was observed in the spectra even for measurements in the regions presenting change in color. Several plausible explanations for these results exist. Firstly, the use of ATR-FTIR as a measurement technique presents a limitation in its surface sensitivity, as it can only probe a thin layer of material, typically around 0.5 and 2 μm [14]. Consequently, if the chemical changes of interest occur deeper within the sample and do not manifest on the surface, they may go undetected. Secondly, it is important to consider

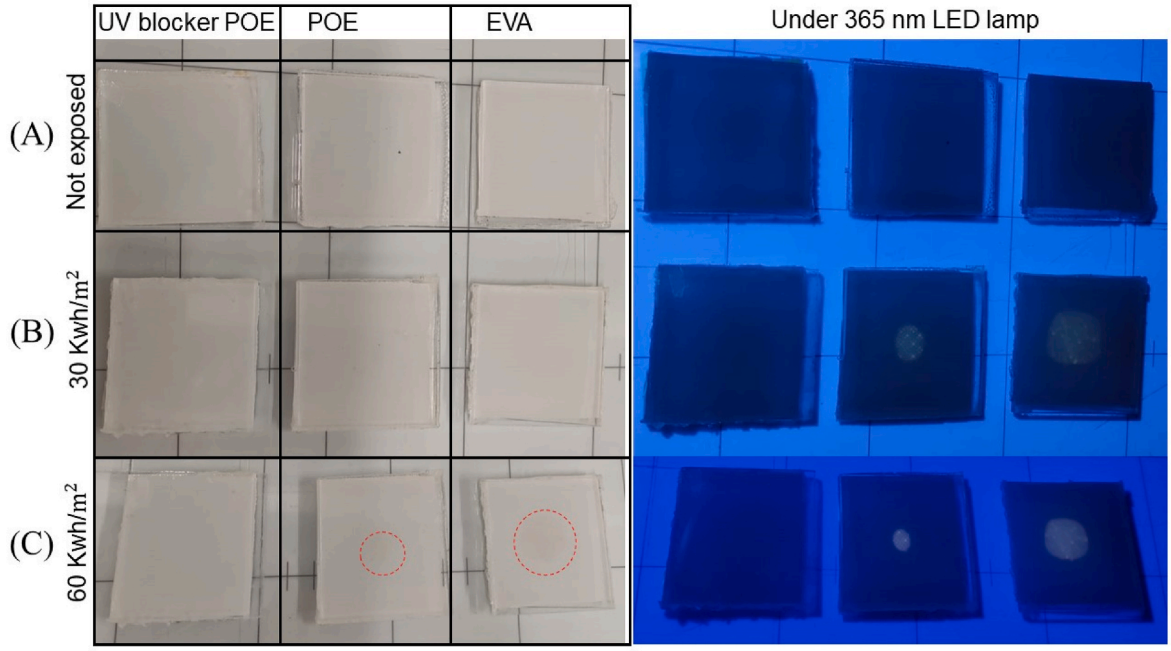

Fig. 4. G/BS laminates with 2-PEA in between the encapsulant layers (see Fig. 1(B)). (A) Not exposed samples show no difference under UV-fluorescence imaging. (B) and (C), 30 kWh/m^2 and 60 kWh/m^2 respectively, highlighted in red dashed lines, a mild yellow color appear in the samples under an ambient light picture (left) and a slight increase in fluorescence is appreciated (right). The UV blocker mitigates the degradation.

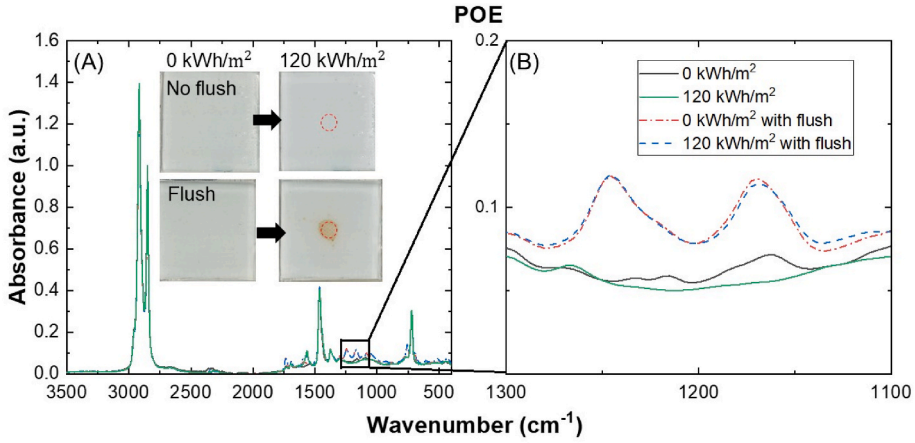

Fig. 5. POE G/BS laminates subjected to exposure of 120 kWh/m^2, both with and without flush, before and after the exposure period. The red circular dashed lines show the region where the encapsulant was extracted. (A) Absorbance spectra from 3500 to 500 cm^{-1} and (B) close up view from 1300 to 1100 cm^{-1} with modified scale showing the peaks corresponding to 2-PEA. The data was normalized at 2850 cm^{-1}.

the composition of the samples. The encapsulant material constitutes the primary component, while the ink components are relatively minor in comparison. As a result, any significant changes in the overall signal would be predominantly influenced by the encapsulant. Therefore, if the encapsulant remains relatively stable and unchanged, it becomes challenging to detect variations due to the limits of detection of the device and the overlapping bands present in the FTIR spectrum. Overall, these factors contribute to the difficulty in detecting certain chemical changes using ATR-FTIR in this context. The measurement's surface sensitivity and the dominant signal from the encapsulant pose challenges when attempting to identify subtle variations or shifts in the ink components.

The pure component of the ink and flush, 2-PEA, polymerized after 1.5 kWh/m^2, and it turned yellow after 15 kWh/m^2. Fig. 6 shows that there is a rise in the 1720 cm^{-1} peak following degradation. This is due to the creation of carbonyl bonds in the substance, which are related to the oxidation of the molecule under UV light [18]. The carbonyl index (CI) was computed as shown in Equation (1), and it rose by 22% following the UV exposure of 15 kWh/m^2. We definitely see an increase in intensity in multiple peaks after degradation, indicating a possible production of carbon double bonds (C═C) throughout the ageing process [19]. The formation of polyconjugated carbon double bonds (C═C)$_n$ and carbonyl groups may be a significant contributory factor to the development of yellowness in the degraded 2-PEA, as it has been observed with other polymers [20–23]. When subjected to the protocol, the 2-PEA component undergoes both polymerization and photodegradation. Consideration can be given to aliphatic monomers as a potential alternative to 2-PEA, as they exhibit superior non-yellowing properties [5].

3.3. Thermo-desorption gas-chromatography coupled to mass spectrometry (TD-GCMS)

The results of TD-GCMS measurements can be seen in Fig. 7(A). The

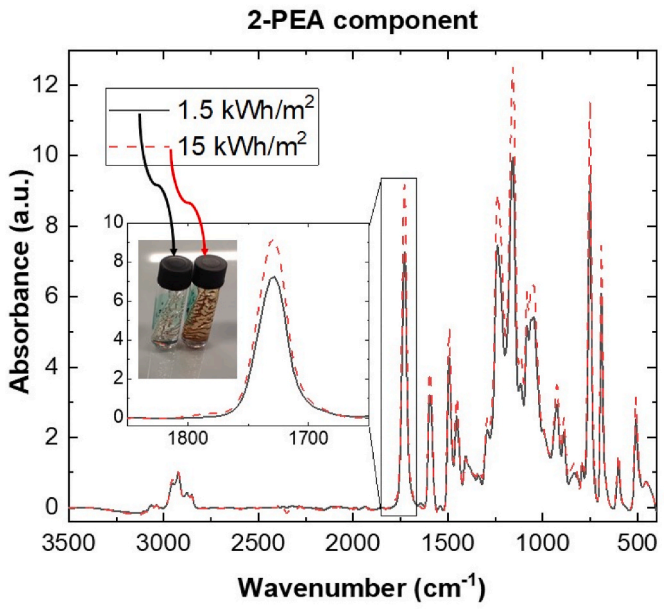

Fig. 6. ATR-FTIR spectra in absorbance mode of the 2-PEA component after 1.5 kWh/m^2 and 15 kWh/m^2 of UV exposure. As it degrades the CI increases and the polymer becomes yellow. The data was normalized at 2850 cm^{-1}.

chromatograms show presence of several peaks corresponding to substances that evolved during the thermo-desorption step from the encapsulants extracted from the G/BS laminates. The samples before the exposure to UV light showed presence of a residue of peroxide at about 6 min, crosslinking accelerator at about 17 min and hindered amine light stabilizer (HALS) at 29.8 min. Additionally, the sample with flush, showed presence of substances below 15 min that can be traced back to 2-PEA. Interestingly, the sample with flush that was exposed to 120 kWh/m^2 did not show presence of HALS, as can be seen in Fig. 7(B). Typically, HALS protect the polymers from photo-oxidation trapping the carbon centered radicals by nitroxyl radicals [24]. In case of the sample laminated with the flush, the HALS might have acted not only to protect the encapsulant from photo-oxidation, but also to contrast the degradation processes taking place in the flush itself, thus accelerating the stabilizer's consumption. It is also possible that the stabilizer migrated during the exposure making the HALS undetectable [25].

3.4. Raman spectroscopy

The Raman spectroscopy measurements are presented in Fig. 8. In order to analyze the peeled G/BS EVA samples with ink coated ribbons, a line scan was conducted across a peeled sample that was not subjected to UV exposure, as well as one after subjecting it to 120 kWh/m^2 of UV exposure. The scan on the sample without exposure encompassed a range extending from the coated metallic interconnect into the encapsulant further away from it, as shown in Fig. 8(B). An interesting observation is the consistent decrease in the intensity ratio between the 1000 and 1065 cm^{-1} peaks as the scan approaches regions further away from the ribbon. These peaks are associated with 2-PEA compound and ethylene units of EVA [26], respectively. This observation suggests that the ink components undergo diffusion into the encapsulant material, resulting in a higher concentration in the immediate proximity of the metallic ribbon and a lower concentration in regions further away. Numerous studies have analyzed the diffusion mechanisms of smaller organic molecules within a cross-linked polymer matrix at elevated temperatures [27,28]. Given the widespread occurrence of this known phenomenon, these findings should not be considered particularly surprising. As for the UV-exposed sample, another line scan was performed. Unfortunately, it was not possible to measure the fully yellow material due to the masking effect of fluorescence, which hides the Raman peaks; therefore, the results are not presented in this work.

3.5. Electrical performance

The electrical performance measurements suggest that the investigated inks do not influence the power output of the modules. There will be reduction in short circuit current (I_{sc}) due to shading losses if the coating is printed on top of the solar cell, but after ageing the loss of power will not increment considerably even with the diffusion of ink components into the encapsulant (see Fig. 9). Besides the IV curve we performed EL measurements, not reported here, that did not show any degradation. Upon UV light exposure the fluorescence from the degraded ink on the PV mini module becomes highly noticeable.

4. Conclusions

In this investigation, the aim was to assess the long-term stability of black-coated metallic ribbons and their possible degradation effects. Three black metallic interconnects coated with different inks and encapsulated in a G/BS configuration were aged under light UV exposure with a protocol based on existing IEC standards. The commercially

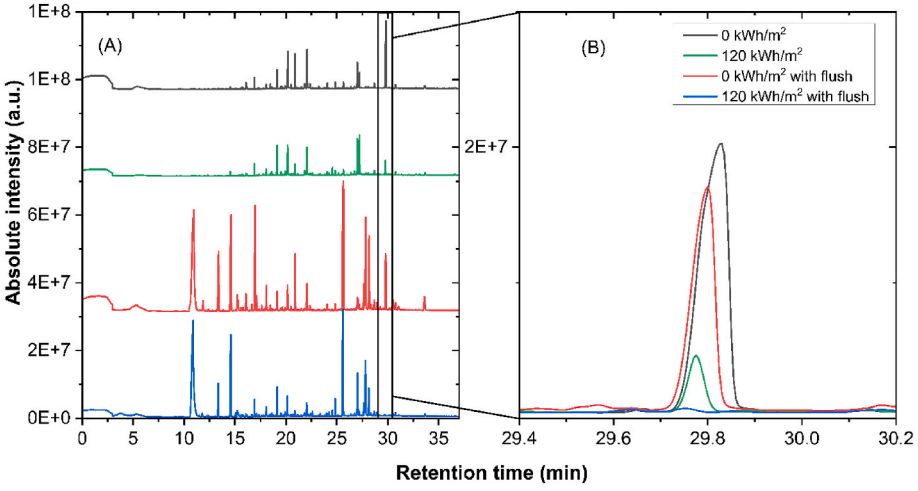

Fig. 7. (A) TD-GCMS chromatograms of EVA extracted from G/BS samples in similar position as shown in the samples of Fig. 5 with and without flush and (B) close up view rescaled from 29.4 min to 30.2 min showing peaks correspondent to hindered amine light stabilizer (HALS).

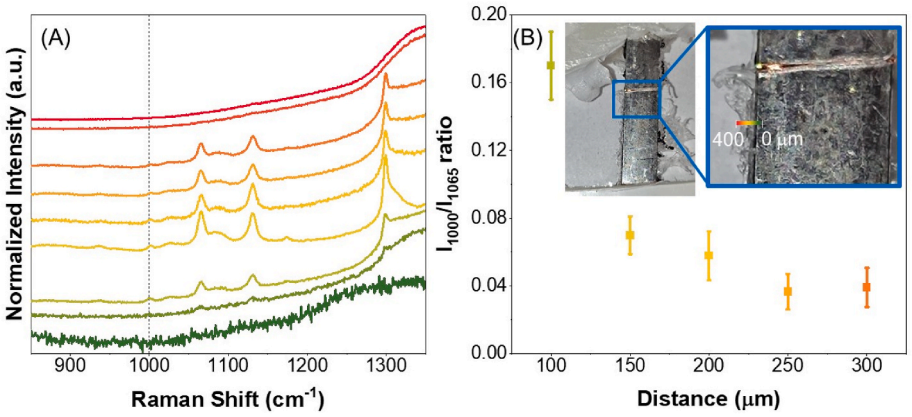

Fig. 8. Raman spectra line scan of the EVA encapsulant inside a G/BS sample with coated ribbon with ink #1 without UV exposure. (A) Normalized intensity of the Raman shift on a line scan from 0 µm, in dark green, to 400 µm, in red. The vertical dashed line highlight the 1000 cm^{-1} peak related to 2-PEA. (B) The ratio between the 1000 and 1065 cm^{-1} peaks decreases as the distance increases, suggesting diffusion of 2-PEA into the encapsulant.

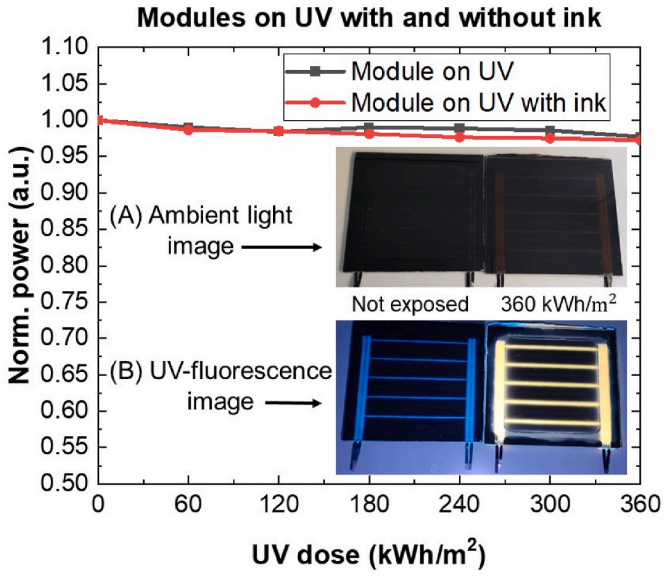

Fig. 9. Normalized power of reference module without coated ribbons and coated module with ink #1 on UV exposure. It is important to note that the measuring equipment used has a reproducibility of ±1%, therefore minimal power loss in both cases is measured. (A) Ambient light image and (B) UV-fluorescence image were captured at two UV exposure levels: 0 kWh/m^2 and 360 kWh/m^2, revealing a significant increase in color change and fluorescence in the ink-coated modules.

available coated ribbons remained stable after 120 kWh/m^2 of UV exposure. This investigation has identified that the studied UV-curable inkjet inks produce color changes in the portion of encapsulant surrounding the coated metallic interconnect. This, irrespective of the encapsulant used, and of the presence or not of UV blockers in the encapsulant. These findings cannot be necessarily generalized to all UV-curable inkjet inks.

In order to explain the observed color changes, we focused our investigation on ink #1, which produced the largest color change, and on its main component 2-PEA. From our observations, the 2-PEA component of the ink is photodegrading and contributing to the observed yellowing. This is proven with the slight increase of 22% in carbon index CI after 15 kWh/m^2 of UV exposure as observed from ATR-FTIR spectra. TD-GCMS measurements revealed that the HALS in the G/BS samples may have served not only to protect the encapsulant from photo-oxidation, but also to contrast the degradation processes taking place in the flush itself, thus accelerating the stabilizer's consumption. A different interpretation is that the stabilizer might have migrated during the exposure, making the HALS imperceptible. The findings of this study suggest that UV blocker encapsulants help mitigating the photo-degradation of 2-PEA on G/BS laminates, whereas they do not fully mitigate the degradation for the ink itself. It is possible, therefore, that other ink components contribute in a larger extent to the color change observed. However, we discourage the use of 2-PEA monomer for PV aesthetic applications and suggest the use of UV curable inks with aliphatic monomers, which have better non-yellowing properties, in combination with UV blocker encapsulants. The study is limited by the lack of information of undisclosed commercial ink components. In spite of its limitations, the study certainly adds to our understanding of the degradation of ink components on PV modules.

Additionally, the metallic ribbons of our one-cell modules were coated with the unstable ink #1 and aged under UV to assess the impact on aesthetics and electrical performance. The use of the investigated unstable ink would represent an aesthetical modification of color in the long-term demonstrating a potential long-term instability, but the electrical performance would be similar to a module without coated ribbons (less than 3% power loss after 360 kWh/m^2 of UV exposure).

A follow-up investigation would be that of designing a specific ink compatible with a commercial coating process for industrial scale PV modules, as no UV curable-inkjet inks made explicitly for coating the metallic interconnects of PV modules are apparently available, and the further study of several solutions provided by the market. This paper contributes to the understanding of the specific requirements needed for these coating layers.

CRediT authorship contribution statement

Alejandro Borja Block: Writing – review & editing, Writing – original draft, Visualization, Validation, Software, Project administration, Methodology, Investigation, Funding acquisition, Formal analysis, Data curation, Conceptualization. **Chiara Barretta:** Writing – review & editing, Writing – original draft, Validation, Methodology, Investigation, Formal analysis, Data curation, Conceptualization. **Antonin Faes:** Writing – review & editing, Visualization, Validation, Supervision, Project administration, Funding acquisition, Conceptualization. **Alessandro Virtuani:** Writing – review & editing, Visualization, Validation, Supervision, Project administration, Funding acquisition, Conceptualization. **Aleš Vlk:** Writing – original draft, Resources, Methodology, Investigation, Formal analysis, Data curation. **Martin Ledinský:** Supervision, Resources, Funding acquisition. **Gernot Oreski:** Writing – review & editing, Visualization, Validation, Supervision, Resources. **Christophe Ballif:** Writing – review & editing, Visualization,

Validation, Supervision, Resources, Funding acquisition.

Declaration of competing interest

The authors declare that they have no known competing financial interests or personal relationships that could have appeared to influence the work reported in this paper.

Acknowledgments

This project has received funding from the European Union's Horizon 2020 research and innovation programme under the Marie Skłodowska-Curie grant agreement No 754354, has been funded in part by the European Commission (EC) and by SERI under the H2020 Be-SMART (#818009) and Horizon Europe Pilatus Project (#101084046). We gratefully acknowledge support from all PV-Lab, PCCL, FZU, and CSEM team members.

References

[1] IEA, Buildings [Online]. Available: https://www.iea.org/reports/buildings, 2022.
[2] R. Renewables now, REN21 - 2022 - Renewables 2022 Global Status Report, 2022.
[3] J. Escarre, et al., When PV modules are becoming real building elements: white solar module, a revolution for BIPV, in: 2015 IEEE 42nd Photovoltaic Specialist Conference (PVSC), IEEE, New Orleans, LA, Jun. 2015, pp. 1–2, https://doi.org/10.1109/PVSC.2015.7355630.
[4] S.A. Awuku, A. Bennadji, F. Muhammad-Sukki, N. Sellami, Myth or gold? The power of aesthetics in the adoption of building integrated photovoltaics (BIPVs), Energy Nexus 4 (Dec. 2021), 100021, https://doi.org/10.1016/j.nexus.2021.100021.
[5] S. Magdassi (Ed.), The Chemistry of Inkjet Inks, World Scientific, Singapore ; Hackensack, NJ, 2010.
[6] A. Hancock, L. Lin, Challenges of UV curable ink-jet printing inks – a formulator's perspective, Pigment Resin Technol. 33 (5) (Oct. 2004) 280–286, https://doi.org/10.1108/03699420410560470.
[7] W. Gambogi, et al., Weathering and durability of PV backsheets and impact on PV module performance, in: N.G. Dhere, J.H. Wohlgemuth, K.W. Lynn (Eds.), Presented at the SPIE Solar Energy + Technology, Sep. 2013, 88250B, https://doi.org/10.1117/12.2024491. San Diego, California, United States.
[8] Terrestrial photovoltaic (PV) modules: design qualification and type approval. Part 2, Test procedures = Modules photovoltaïques (PV) pour applications terrestres : qualification de la conception et homologation. Partie 2, Procédures d'essai, second ed..0, 2021.
[9] A. Borja Block, A. Virtuani, C. Ballif, Stability of inks used for masking metallic interconnects in BIPV modules, in: 38th Eur. Photovolt. Sol. Energy Conf. Exhib., 723–727, 2021, p. 5, https://doi.org/10.4229/EUPVSEC20212021-4AV.1.11, 4767 kb.
[10] C.H. Schiller, S. Hoffmann, M. Jahn, A. De Rose, M. Heinrich, Fully black and reliable PV modules with a cost-effective inkjet coating of cell strings, in: 8th World Conf. Photovolt. Energy Convers., 790–796, 2022, p. 7, https://doi.org/10.4229/WCPEC-82022-3DV.1.1, 7429 kb.
[11] A. Borja Block, J. Escarre Palou, A. Faes, A. Virtuani, C. Ballif, A screening protocol to assess the stability of inks used to mask metallic interconnects in BIPV modules, in: 8th World Conf. Photovolt. Energy Convers., 902–906, 2022, p. 5, https://doi.org/10.4229/WCPEC-82022-3DV.3.15, 4780 kb.
[12] IEC TS 62788-7-2: Measurement Procedures for Materials Used in Photovoltaic Modules - Part 7-2: Environmental Exposures - Accelerated Weathering Tests of Polymeric Materials, International Electrotechnical Commission, 2017.
[13] G. Sharma, W. Wu, E.N. Dalal, The CIEDE2000 color-difference formula: implementation notes, supplementary test data, and mathematical observations, Color Res. Appl. 30 (1) (Feb. 2005) 21–30, https://doi.org/10.1002/col.20070.
[14] Y. Lyu, et al., Fluorescence imaging analysis of depth-dependent degradation in photovoltaic laminates: insights to the failure, Prog. Photovoltaics Res. Appl. 28 (2) (Feb. 2020) 122–134, https://doi.org/10.1002/pip.3212.
[15] R. Satoto, W.S. Subowo, R. Yusiasih, Y. Takane, Y. Watanabe, T. Hatakeyama, Weathering of high-density polyethylene in different latitudes, Polym. Degrad. Stabil. 56 (3) (Jun. 1997) 275–279, https://doi.org/10.1016/S0141-3910(96)00213-3.
[16] M.S. Salim, D. Ariawan, M.F. Ahmad Rasyid, R. Mat Taib, M.Z. Ahmad Thirmizir, Z.A. Mohd Ishak, Accelerated weathering and water absorption behavior of kenaf fiber reinforced acrylic based polyester composites, Front. Mater. 7 (Feb. 2020) 26, https://doi.org/10.3389/fmats.2020.00026.
[17] G. Oreski et al., "Reliability of Electrically Conductive Adhesives," presented at the 35th European Photovoltaic Solar Energy Conference and Exhibition, [Online]. Available: https://www.eupvsec-proceedings.com/proceedings?fulltext=p%C3%B6tz&paper=46359.
[18] C. Decker, K. Zahouily, Photodegradation and photooxidation of thermoset and UV-cured acrylate polymers, Polym. Degrad. Stabil. 64 (2) (May 1999) 293–304, https://doi.org/10.1016/S0141-3910(98)00205-5.
[19] F. Liu, L. Jiang, S. Yang, Ultra-violet degradation behavior of polymeric backsheets for photovoltaic modules, Sol. Energy 108 (Oct. 2014) 88–100, https://doi.org/10.1016/j.solener.2014.06.027.
[20] F. Pern, A. Czanderna, Characterization of ethylene vinyl acetate (EVA) encapsulant: effects of thermal processing and weathering degradation on its discoloration, Sol. Energy Mater. Sol. Cells 25 (1–2) (Jan. 1992) 3–23, https://doi.org/10.1016/0927-0248(92)90013-F.
[21] G. Oreski, G.M. Wallner, Evaluation of the aging behavior of ethylene copolymer films for solar applications under accelerated weathering conditions, Sol. Energy 83 (7) (Jul. 2009) 1040–1047, https://doi.org/10.1016/j.solener.2009.01.009.
[22] A. Krauklis, A. Echtermeyer, Mechanism of yellowing: carbonyl formation during hygrothermal aging in a common amine epoxy, Polymers 10 (9) (Sep. 2018) 1017, https://doi.org/10.3390/polym10091017.
[23] J. Segurola, N.S. Allen, M. Edge, A. McMahon, S. Wilson, Photoyellowing and discolouration of UV cured acrylated clear coatings systems: influence of photoinitiator type, Polym. Degrad. Stabil. 64 (1) (Apr. 1999) 39–48, https://doi.org/10.1016/S0141-3910(98)00169-4.
[24] N.S. Allen, M. Edge, Perspectives on additives for polymers. Part 2. Aspects of photostabilization and role of fillers and pigments, J. Vinyl Addit. Technol. 27 (2) (May 2021) 211–239, https://doi.org/10.1002/vnl.21810.
[25] G. Haacke, F.F. Andrawes, B.H. Campbell, Migration of light stabilizers in acrylic/melamine clearcoats, JCT J. Coat. Technol. 68 (1996) 57–62.
[26] C. Peike, T. Kaltenbach, K.-A. Weiß, M. Koehl, Non-destructive degradation analysis of encapsulants in PV modules by Raman Spectroscopy, Sol. Energy Mater. Sol. Cells 95 (7) (Jul. 2011) 1686–1693, https://doi.org/10.1016/j.solmat.2011.01.030.
[27] A. Ahmad, S.-H. Li, Z.-P. Zhao, Insight of organic molecule dissolution and diffusion in cross-linked polydimethylsiloxane using molecular simulation, J. Membr. Sci. 620 (Feb. 2021), 118863, https://doi.org/10.1016/j.memsci.2020.118863.
[28] B. Mei, T.-W. Lin, G.S. Sheridan, C.M. Evans, C.E. Sing, K.S. Schweizer, How segmental dynamics and mesh confinement determine the selective diffusivity of molecules in cross-linked dense polymer networks, ACS Cent. Sci. 9 (3) (Mar. 2023) 508–518, https://doi.org/10.1021/acscentsci.2c01373.